Geophysical Research Letters

RESEARCH LETTER
10.1029/2018GL080866

Insights Into Fault-Magma Interactions in an Early-Stage Continental Rift From Source Mechanisms and Correlated Volcano-Tectonic Earthquakes

S. J. Oliva[1], C. J. Ebinger[1], C. Wauthier[2,3], J. D. Muirhead[4], S. W. Roecker[5], E. Rivalta[6], and S. Heimann[6]

[1]Tulane University, New Orleans, LA, USA, [2]Pennsylvania State University, University Park, PA, USA, [3]Institute for CyberScience, University Park, PA, USA, [4]Syracuse University, Syracuse, NY, USA, [5]Rensselaer Polytechnic Institute, Troy, NY, USA, [6]GFZ German Centre for Geosciences, Potsdam, Germany

Key Points:
- Non-double-couple earthquakes are observed in an early-stage rift and interpreted as fluid-involved faulting above a sill complex
- Earthquakes in 2013–2014 have similar driving mechanisms as the fault-dike-eruption episode in 2007–2008 but did not rupture the same faults
- Magma-involved faulting persistently accommodates strain over intereruptive cycles

Supporting Information:
- Supporting Information S1

Correspondence to:
S. J. Oliva,
soliva@tulane.edu

Citation:
Oliva, S. J., Ebinger, C. J., Wauthier, C., Muirhead, J. D., Roecker, S. W., Rivalta, E., & Heimann, S. (2019). Insights into fault-magma interactions in an early-stage continental rift from source mechanisms and correlated volcano-tectonic earthquakes. *Geophysical Research Letters*, *46*. https://doi.org/10.1029/2018GL080866

Received 10 OCT 2018
Accepted 5 FEB 2019
Accepted article online 12 FEB 2019

©2019. American Geophysical Union. All Rights Reserved.

Abstract Strain in magmatic rifts is accommodated by both faulting and dike intrusion, but little is known of the frequency of dike intrusions in early-stage rifts. We use a new earthquake data set from a dense temporary seismic array (2013–2014) in the ~7-Myr-old Magadi-Natron-Manyara section of the East African Rift, which includes the carbonatitic Oldoinyo Lengai volcano that erupted explosively in 2007–2008. Full moment tensor analyses were performed on $M > 3.4$ earthquakes (0.03- to 0.10-Hz band) that occurred during the intereruptive cycle. We find two opening crack-type and various non-double-couple earthquake source mechanisms and interpret these as fluid-involved fault rupture. From waveform analysis on the nearest permanent seismic station, we conclude that similar rupture processes probably occur over eruptive and intereruptive cycles. The repeated and dynamically similar fluid-involved seismicity, along with intrabasinal localization of active deformation, suggests that significant and persistent strain is accommodated by magmatic processes, modulated by tectonic cycles.

Plain Language Summary How do Earth's plates deform between volcanic eruptions and after plate tectonic stresses have been released in large earthquakes? Simulations of earthquake rupture in rift zones where the plates are diverging tell us that opening + shearing cracks created several of the moderate earthquakes. The opening may be due to magmatic fluids and gases from crustal magma reservoirs. We also compare the earthquake signals to those from the past 20 years and find that these magma-related earthquakes are frequent occurrences at least in the past 10 years. Magmatic processes contribute to the short time scale cycles of plate boundary deformation in rift zones.

1. Introduction

Crustal extension within active continental rift zones is accommodated by faulting and dike intrusion, but the timing and length scales of magma intrusion remain weakly constrained. Although the magma intrusion itself is aseismic, the rocks adjacent to intrusions experience failure, potentially due to gases exsolving and causing fluid-driven fracturing in the solid rock (e.g., Rubin, 1995). Fault rupture and related seismicity may also result from stress concentrations around the edges of blade-shaped propagating dikes (e.g., Belachew et al., 2011; Bonafede & Danesi, 1997). However, it remains unclear whether dike-related seismicity results from stressed, intact rock failing above and below the dikes without effects from fluid percolation (e.g., Rowland et al., 2007) or whether the earthquake rupture initiates in rock with magma-filled cracks (e.g., Belachew et al., 2013; Rubin, 1995). The latter's source mechanism would have a dilatational component due to the magma and gas inflation along the fault zone (Belachew et al., 2013; Minson et al., 2007), whereas the former would result in a double-couple (DC) mechanism (e.g., Ágústsdóttir et al., 2016). Identification of characteristic source mechanisms of dike intrusions enables assessment of the frequency of magma intrusions in rift zones and their relationship to magmatic and tectonic stressing cycles (e.g., Ebinger et al., 2013).

The aim of our earthquake source mechanism study of the largest earthquakes ($3.4 < M_L < 4.7$) during an intereruptive rifting cycle is to evaluate the role of magma in strain accommodation by allowing for dilatation in our earthquake source models. We obtain full moment tensors from a new earthquake data set from a dense temporary seismic array in the Magadi-Natron-Manyara rift segments of the Eastern rift,

East Africa (Weinstein et al., 2017), which includes the only currently active carbonatitic volcano, Oldoinyo Lengai, which last erupted explosively in 2007–2008 (e.g., Calais et al., 2008). Whereas full moment tensor analysis of earthquakes is becoming common, few studies consider statistical analysis of solution robustness (e.g., Alvizuri et al., 2018; Silwal & Tape, 2016; Stähler & Sigloch, 2014). In this study, we perform uncertainty analysis of source mechanisms via the bootstrap method (Efron, 1992; Rubin, 1981). Since similar earthquake waveforms arise from repeated slip on the same fault patch (e.g., Marone et al., 1995; Waldhauser et al., 2004), comparisons of waveforms from permanent station IU-KMBO (Albuquerque Seismological Laboratory/USGS, 1988) allow us to investigate preeruptive, eruptive, and intereruptive events over the past 22 years in this early-stage rift sector (e.g., McNutt, 2005; Tepp et al., 2016).

2. Background

The East African Rift System extends from the Afar triple junction in the north to Mozambique and Madagascar in the south and southeast to Botswana in the southwest (Ebinger et al., 1997; Modisi et al., 2000). The Magadi-Natron-Manyara region is the most seismically active sector of the Eastern Rift, and major faults and magmatism developed after ~7 Ma (Ashley, 2007; Mana et al., 2012, 2015; Muirhead et al., 2016; Figure 1). Rigid plate models of earthquake focal mechanisms and permanent Global Positioning System data indicate a N110°E extension direction at <5 mm/year (Albaric et al., 2014; Saria et al., 2013, 2014; Weinstein et al., 2017). Receiver function studies reveal 40-km-thick crust thinned to 29 km beneath the Natron rift basin (Plasman et al., 2017), consistent with controlled source estimates beneath the Magadi basin (Birt et al., 1997). Both experiments indicate a thick zone of magmatic underplate beneath the rift basins (Birt et al., 1997; Plasman et al., 2017), and large volumes of magmatic gas emissions along border faults indicate that the intrusion process is ongoing across a broad region (Lee et al., 2016).

Late Miocene-Recent eruptive centers occur along the flanks of the Magadi-Natron rift zone, and carbonatitic, basaltic, and monogenetic eruptive centers occur within the fault-bounded half-graben (Mana et al., 2015; Muirhead et al., 2016; Figure 1). In 2007, the south Natron basin was the site of an earthquake swarm and a large volume dike intrusion beneath the Naibor Soito (NS) monogenetic cone complex and southern flank of the Gelai volcano and a subsequent explosive eruption at the carbonatitic Oldoinyo Lengai (OL) volcano (Baer et al., 2008; Biggs et al., 2009; Calais et al., 2008; Kervyn et al., 2010). Although no surface ruptures were identified from the initial M_w5.9 earthquake, Interferometric Synthetic Aperture Radar (InSAR) and global Centroid Moment Tensor (CMT) source models suggest a 45° NW dipping fault (Biggs et al., 2009, 2013; Calais et al., 2008; Wauthier, 2011). The M_w5.9 earthquake was followed 6 days later by a <2-m-wide, ~8-km-long diking event that produced a 2- to 3-km-wide graben, although the location of the pressurized magma chamber(s) from which the dike was fed is debated (Biggs et al., 2009; Calais et al., 2008). The sequence was closely followed by a 9-month-long eruption at Oldoinyo Lengai, suggesting that the fault-dike sequence triggered the eruption (e.g., Baer et al., 2008). Interpretations of new geophysical, geochemical, and structural data motivate reanalyses of the 2007 sequence, indicate pressurized sills and magma chambers, and provide new insights into rifting dynamics.

Earlier work on focal mechanisms reveal local rotation to NNW-SSE extension direction in the OL-NS-Gelai volcanic area, but only focal mechanisms based on first-motion polarities were considered (Weinstein et al., 2017). The global CMT catalog, which assumes no isotropic component, reports CMTs from the 2007 episode (Ekström et al., 2012). When seismic events besides simple faulting are expected in a region of study (e.g., in volcanic areas), it is important to consider that different source types and source decompositions might fit the data when making interpretations (Cesca et al., 2017; Nettles & Ekström, 1998). In this study, we obtain full moment tensor (FMT) solutions to probe processes that caused the seismic events, as opposed to the focal mechanisms reported in Weinstein et al. (2017) which only represent the DC solution and global CMTs which are deviatoric (DC + compensated linear vector dipole, CLVD) solutions that do not allow an isotropic component (Dahm & Krüger, 2014; Jost & Herrmann, 1989; see Text S1 in the supporting information).

3. Data and Methods

In this part of Africa, permanent seismic stations are sparse. The longest-running (active since 1995 to present) and nearest permanent seismic station is IU-KMBO located in Nairobi, Kenya, about 220 km from

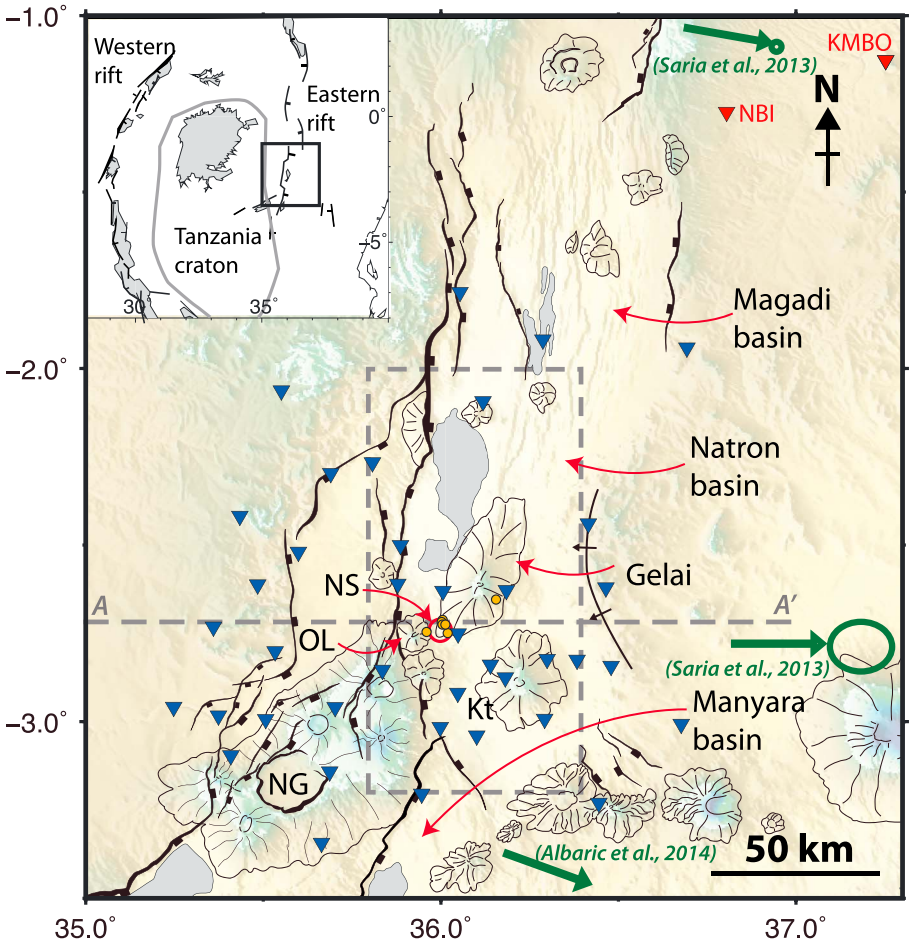

Figure 1. Map of the Magadi-Natron-Manyara region. Light lines enclose the edifices of <7-Myr-old volcanoes (Mana et al., 2015). The 2013–2014 CRAFTI array (blue inverted triangles) encloses the Naibor Soito monogenetic cone complex (NS) located between the active carbonatitic Oldoinyo Lengai volcano (OL) and the dormant Gelai volcano. The OL-NS-Gelai complex was host to a seismomagmatic crisis in July–August 2007 that included a diking event in Naibor Soito and an eruption at Oldoinyo Lengai. Waveforms from the permanent station IU-KMBO (red triangle, northeast corner) are used to study the seismic activity beyond the duration of the local array. Green arrows with error ellipses are extension directions derived from Global Positioning System (Saria et al., 2013) and focal mechanisms (Albaric et al., 2014; Weinstein et al., 2017). Faults and edifices adapted from Muirhead et al. (2015). Orange circles are the seven earthquakes studied (Figure 2). The dashed box shows the extent of Figures 2 and 3. Figure 4 shows the cross section along A-A′. Kt = Kitumbeine; NG = Ngorongoro crater.

Naibor Soito (Figure 1, red triangle). Seismic waveforms from IU-KMBO were obtained for 253 events in the area reported by Incorporated Research Institutions for Seismology Data Management Center since 1995. AfricaArray station AF-NBI was also nearby but only ran in 2011–2015. In part to fill this data gap, 39 broadband seismic stations were deployed in 2013–2014 around the Magadi-Natron-Manyara sector of the Eastern rift (Weinstein et al., 2017; Figure 1, blue triangles). Earthquakes with $M_L > 3.4$, good azimuthal coverage (<120° gap), and high-quality waveforms from the Weinstein et al. (2017) catalog were chosen for full waveform analyses, performed using the Time-Domain Moment Tensor Inverse Code (TDMT_INVC; Dreger, 2003; Ford et al., 2009; Minson & Dreger, 2008; Saikia, 1994) and the Grond package (Heimann et al., 2017, 2018; Wang, 1999) using a 1-D velocity model (Roecker et al., 2017) and density relations (Brocher, 2005) (see Texts S2 and S3 and Table S1). In TDMT_INVC, we use long-period waves (0.03–0.10 Hz), assume a spatial and temporal point source to linearize the moment tensor problem, and perform a 1-km grid search over depth to find the best solution (Pasyanos et al., 1996). Robustness of source mechanism solutions is investigated using a Bayesian bootstrap method where weights of individual stations are varied at random (e.g., Dahm et al., 2018; see Text S2). The 2007 teleseismically detected earthquakes

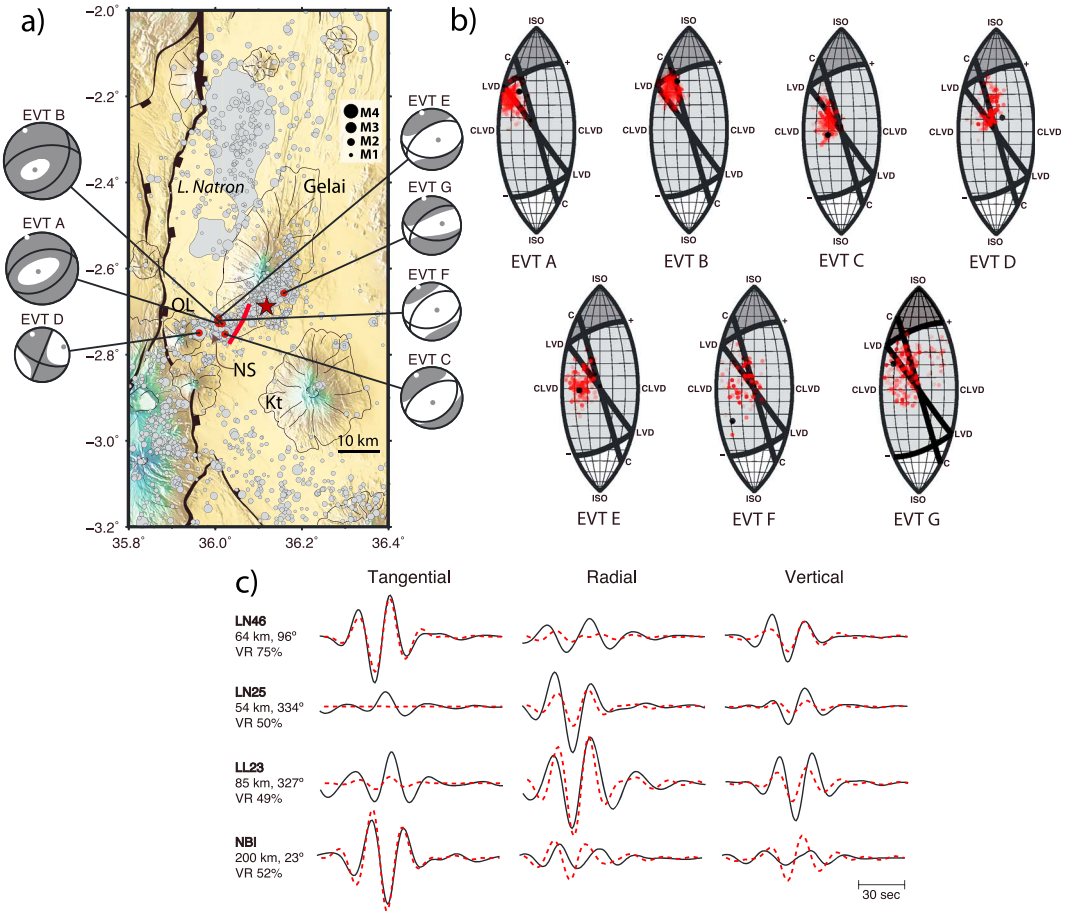

Figure 2. Full moment tensors. (a) Notable are the two *M*4.7 earthquakes on 3 June 2013 (Events A and B) that occurred within close proximity in time and space and with very similar source mechanisms. The local seismicity recorded by the 2013–14 local network are plotted as gray dots (magnitude scale in black). The red line represents the 2007 dike; the red star is the 2007 M_w5.9 earthquake. (b) Bootstrap results plotted on the lune source-type plot (Tape & Tape, 2013) show robustness of source mechanisms for Events A–E, where red dots are the bootstrap solutions and the black dot is the best solution as determined by variance reduction (see Text S3 for details). Labels refer to end-member source mechanisms: ISO = isotropic; C = tensile crack; LVD = linear vector dipole; CLVD = compensated linear vector dipole. Double couple is at the center of the line plot. The list of moment tensor solutions is provided in Table S2. (c) Sample waveform fits (red dashed lines: synthetic waveforms) for Event A are plotted on top of data (solid black lines). Source-to-receiver distance, azimuth, and variance reduction are reported for each station.

have poorly determined locations (e.g., Ekström et al., 2012), but the waveforms recorded at IU-KMBO can be cross-correlated with those from well-located earthquakes of the 2013–2014 data set to evaluate the possible role of magma intrusion in strain accommodation (Reyes & West, 2011; see Text S4).

4. Results

The seven new FMT solutions correspond to earthquakes from the center of the 2013–2014 seismic array (Figures 2 and S1–S8). None of these earthquakes is reported in the global CMT catalog (Ekström et al., 2012). Moment tensor inversion of the seven events provides solutions with variance reduction values of >40% (see Text S3 and Table S2). In-rift stations (e.g., Figure S2—PR33, MW36, LN26, LN25, and LN15) tend to have larger recorded amplitudes than predicted, compared to the flank stations (e.g., Figure S2—NG56, LN46, LN14, and LL23), due to rift-focusing effects. The low variance reduction values could be due to the inadequacy of the model to capture waveform complexity arising from rift effects. All MTs have a NW to NNW trending tension (*T*) axis, with six of the seven having a normal DC component. Event D is located between Oldoinyo Lengai and Naibor Soito monogenetic cone complex; Event G is on the southeast flank of Gelai, whereas the rest of the events are within the Naibor Soito area.

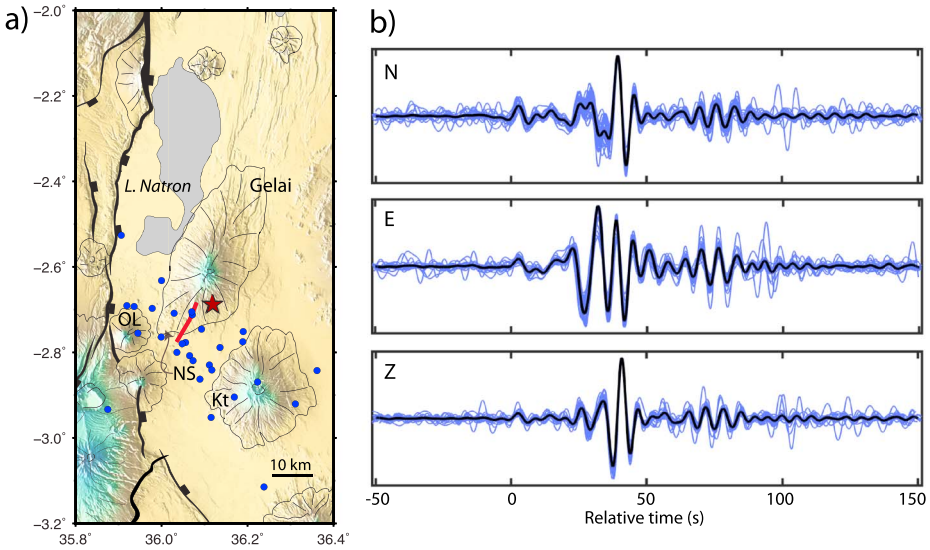

Figure 3. Correlated volcano-tectonic earthquakes. From relative *S-P* times of regional earthquakes recorded at station IU-KMBO, we identify a subset of earthquakes that could have all happened within an arc of radius ±8 km (see Text S5). By cross-correlating the three-component earthquake waveforms band-pass filtered (0.05–0.2 Hz) to the frequency range used in the moment tensor inversion, we find 31 earthquakes that correlate to >80% similarity at all three components (N, E, and Z). (a) The earthquakes are plotted using the National Earthquake Information Center locations, but location errors can be ~26 km based on analyses from Weinstein et al. (2017), due to the sparse network of permanent seismic stations in this area of the world. Faults, volcanic edifices, the 2007 dike (red line), and the 2007 M_w5.9 earthquake (red star) are shown as in Figure 2. (b) The three components of the 31 normalized waveforms (blue) and the stacked waveform (black) are plotted relative to the *P* arrival. The earthquakes are listed in Table S3.

Using a bootstrap-based probabilistic method to explore the moment tensor solution space and assuming full confidence in local catalog locations (allowing only <3-km depth discrepancies), we confirm robust source mechanisms as plotted on the source-type Lune plot (Tape & Tape, 2013; Figure 2b). Events A and B are most tightly constrained to a source type that has a significant isotropic component and plots between crack type and linear vector dipole. Events C and E have primarily deviatoric sources (CLVD+DC) with little isotropic component. Event D is a strike-slip earthquake with some similarity to crack type and LVD but with negligible isotropic component. The results of the bootstrap method for Events F and G show a wider distribution of possible source-type solutions. Note that the least robust solution does not come from the earthquake of smallest magnitude, suggesting that solution robustness is not simply an artefact of the signal-to-noise ratio.

Notable are two M_L4.7 earthquakes (Events A and B) that occurred within 6 hr of each other on 3 June 2013. These occurred when the GPS clocks on many stations failed (Weinstein et al., 2017); nonetheless, the waveforms with timing errors could still be fitted, after manual time corrections. Source mechanisms from these two events are nearly identical, strike northeast, and have source depths of 7–8 km (see Table S2).

Of the 253 earthquakes at OL-NS-Gelai recorded by IU-KMBO in Kenya since 1995 to 2017, band-pass filtered (0.05–0.2 Hz) at the frequencies used in the moment tensor inversion, we find 29 events with seismic waveforms that match the two well-located 2013 earthquakes or 31 in total (Figure 3). These 31 similar events have >80% correlation on the horizontals and >90% correlation on the vertical component within a 100-s window after the first *P* arrival. The majority of these earthquakes are from the July to August 2007 fault-dike-eruption sequence. Two other earthquakes—on 10 July 2008 and 1 April 2010—also belong to the correlated group but were previously not analyzed in detail as there was no local array to study them. Five of these 31 appear in the global CMT catalog (three strongly DC, two with significant CLVD, and all NNW-SSE extension), and the source-type discrepancy between the deviatoric global CMTs and our crack-type FMTs, despite good waveform cross correlation, might be due to regional MTs constraining the non-DC components better than global CMTs.

5. Discussion

5.1. Reliability and Solution Uncertainty

The excellent azimuthal coverage of the local array allows us to assess and quantify solution reliability and errors. The seven earthquakes analyzed in this study span the intereruptive and interseismic cycle, which we assume started after the 2007 M_w5.9 earthquake and 2007–2008 Oldoinyo Lengai eruption. Not all earthquakes in the OL-NS-Gelai complex analyzed in this study have a strong isotropic component, which confirms that there is no bias due to station geometry or local site effects that produce spurious non-DC components (e.g., Panza & Saraò, 2000). The locations reported by the National Earthquake Information Center for the 3 June 2013 Events A and B differed by 23 and 7 km (horizontal) compared to the well-constrained CRAFTI database, highlighting the extent of location inaccuracies typical of regions with sparse permanent station coverage (Weinstein et al., 2017). This is important to consider since moment tensor inversion relies on precise source locations and is limited by station coverage. In this study, local earthquake locations are well constrained, and distribution of bootstrap solutions confirms the robustness of the source mechanisms, at least for the well-constrained Events A–E (Figure 2b).

5.2. Source Interpretation and Processes

The source mechanisms obtained in this study are interpreted in light of other geophysical and field observations. The seven earthquakes all occur at depths 7–11 km, which coincides with two vertically stacked, pancake-shaped earthquake clusters at 6–11 km, imaged and interpreted by Weinstein et al. (2017) as a pressurized sill complex, consisting of layers of sills interconnected via dikes (Figure 4). The non-DC source mechanisms could therefore be indicative of magmatic fluids that percolate up faults during rupture, consistent with measurements of active magmatic CO_2 degassing along fissures and fault traces in the region (Lee et al., 2016; Muirhead et al., 2016). Events A and B occurred near the edges of the interpreted sills, and they have vertical *P* (compression axis) crack-type sources consistent with subvertical cracks (see Figure 4) and could be associated with faulting occurring with bursts of magmatic movement and gas release or hydraulic fracture (e.g., Belachew et al., 2013; Shuler et al., 2013). These crack-type MTs reveal a Poisson's ratio of ~0.28 which is consistent with slightly higher *Vp*/*Vs* ratios detected beneath the rift axial valley (see Text S6; Plasman et al., 2017; Roecker et al., 2017). Events C and E and F, possibly located along a vertical conduit between the sill complex and the underlying lower crustal magma chamber (see Figure 4), have vertical *P* deviatoric to DC sources. The source mechanisms are consistent with fluid transport from a horizontal tensile crack to a vertical cylinder (Shuler et al., 2013) and may be caused by stress adjustments in response to local inflation-deflation cycles and tectonic stressing (e.g., Minson et al., 2007; Shuler et al., 2013). The strike-slip earthquake (Event D), located between the NS complex and the OL plumbing system, could be related to stress adjustments along the sides of the sill complex or fault linkage.

The source mechanisms are oblique to the regional tectonic stress direction and parallel to mechanisms from the 2007 dike intrusion. The ~10-year record of seismicity points to a local stress field rotation, possibly due to a pressurized sill complex above a broad, lower crustal zone of magma intrusion, and storage (Roecker et al., 2017; Weinstein et al., 2017). The non-DC components represent magmatic fluids dilating intrabasinal faults, in a process we refer to as magma-involved faulting.

5.3. Fault and Magma Cycles

Source mechanisms of the largest earthquakes during the interseismic cycle indicate magma-involved faulting, but are the magmas sourced from the same region(s) as the intense 2007–2008 intrusive-eruptive events? Five of the seven earthquakes occurred 2–5 km west of the fissures and collapse structures that formed above the 2007 dike (Muirhead et al., 2016; Figure 2a). The sill-related seismicity is located on the SW tip of the 2007 dike, which could indicate that the dike was sourced from the sill complex, possibly with some lateral magma transport as is seen in high-resolution reflection data from ancient rift basins (e.g., Magee et al., 2016).

We focus our discussion on Events A and B, which have the most well-constrained solutions and show a crack-type source. Cross correlation suggests that the 31 events, corresponding to 28% of the total seismic moment of the 253 events, have similar long-period seismic radiation patterns. Analyzing one station can only confirm seismic radiation similarity along one azimuth, but integrating this result with other information on the region—geological setting, the 2007 tectonomagmatic sequence, and the spatiotemporal

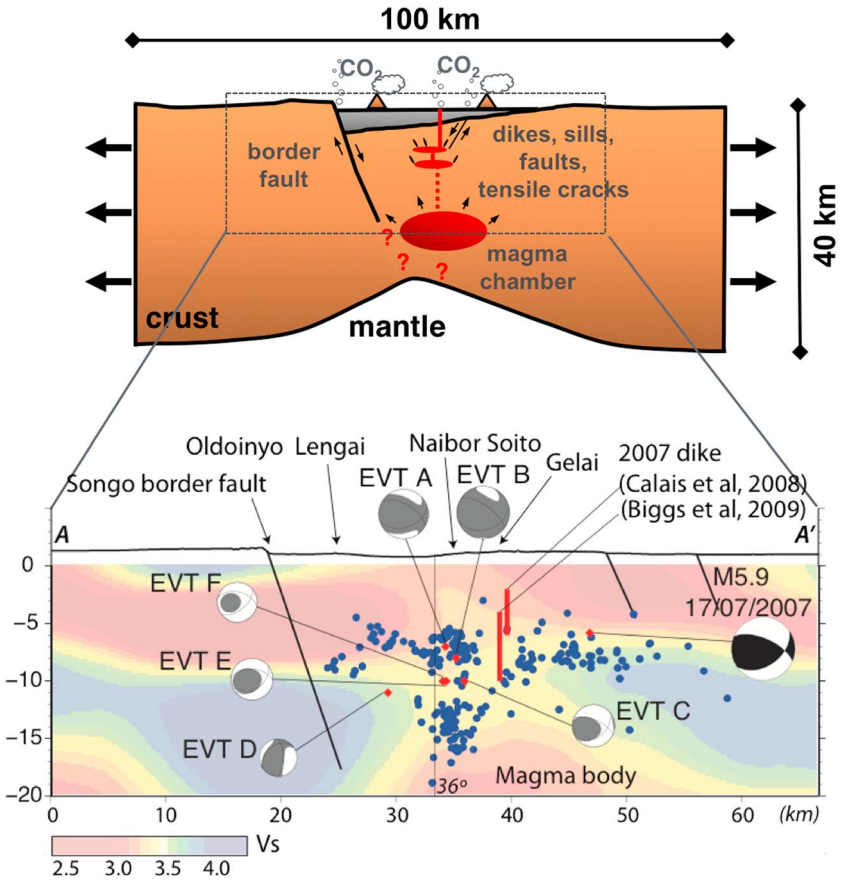

Figure 4. Schematic diagram of rift kinematics. A sill complex (Roecker et al., 2017; Weinstein et al., 2017) provides a local stress field that introduces a stress rotation from the regional extension direction and hosts regional earthquakes of similar mechanisms. These regional earthquakes occur across a swath of faults and tensile cracks above the sills and respond to regional extension, as well as inflation-deflation from the underlying magma chamber. The cross section below shows the double-differenced earthquakes from 2013 to 2014 (Weinstein et al., 2017) located 5 km north and south of A-A′ (see Figure 1, longitude 35–37°, latitude 2.72°). The earthquakes delineate the sill complex and the top of the magma chamber and are plotted on a shear velocity tomography map (Roecker et al., 2017). The 2007 mainshock is also shown, along with the location of the 2007 dike as modeled by two different InSAR studies (Biggs et al., 2009; Calais et al., 2008).

distribution of earthquakes—could imply common rupture mechanisms and suggest similar driving mechanisms. The similar mechanisms may mean that fault-magma interaction occurs even during intereruptive cycles when there is no surface expression of volcanism and no detectable InSAR surface deformation (Wauthier et al., 2016). These crack-type earthquake sources that are persistent in time could be due to (1) gas release that breaks rock, associated to bursts of magmatic intrusion or inflation, or (2) fault slip driven by gas release and percolation up the fault. Despite the differences, the common source mechanisms indicate that rupture occurred in a magma-rich zone, either accompanied by observed magmatism or showing crack-type source mechanisms interpreted as magmatic fluids.

Although cross correlation of the 31 events suggests similar mechanisms, the varying *S-P* arrival times indicate rupture of multiple faults. The lack of correlation at high frequencies (>1 Hz) may be caused by slight differences in earthquake locations based on *S-P* times from IU-KMBO waveforms (see Text S5). The "similar source" earthquakes observed in our study behave differently in that (1) they occur along intrabasinal faults far from the border faults, suggesting greater magma control versus border fault control on strain accommodation (e.g., Ebinger & Casey, 2001; Muirhead et al., 2016) and (2) they are likely due to rupture and slip of multiple faults and tensile cracks responding to the superposition of regional extension and local body forces from low-density magma bodies (Figure 4). Baer et al. (2008) arrived at a similar conclusion of multiple faults for the 2007 fault-dike-eruption sequence, inferred from modeling and fitting InSAR observations. The repeated and dynamically similar magma-involved earthquakes and the localization of active

deformation within intrabasinal magmatic zones suggest that magma intrusion accommodates a significant proportion of rift-related strain during even the early stages of rifting in some rift sectors (e.g., Wauthier et al., 2015). Similarities to strain patterns in 12- to 18-Myr-old mature rift sectors in Ethiopia suggest that we are capturing in Magadi-Natron the early transitions from fault-controlled to magma-controlled rifting (Ebinger & Casey, 2001; Keir et al., 2006; Muirhead et al., 2016).

6. Conclusions

We find magma-related earthquakes in the Natron basin of the East African Rift that are possibly persistent in time, occurring over a small spatial scale, and have similar source mechanisms. They occur above an interpreted sill-magma chamber complex that causes a local stress field rotation and that facilitates magma transport beneath a rift basin (Muirhead et al., 2015; Weinstein et al., 2017). These volcano-tectonic earthquakes correlate very well at low frequencies, suggesting similar source mechanisms, but not at high frequencies, suggesting slight deviations in wave path and location. The non-DC components of these volcano-tectonic earthquakes are interpreted as fluids percolating on a set of slipping faults above a sill complex. We reinterpret the 2007 diking event as having been sourced at least in part from the midcrustal sill complex above a broad zone of lower crustal magma intrusion as imaged by Roecker et al. (2017). The similarities between earthquakes that occurred during a large-volume dike intrusion and subsequent earthquakes indicate that dilatational MTs may be diagnostic of rift zone magma intrusion, and the time sequence may indicate that magma intrusion occurs throughout the rift deformation cycle.

Acknowledgments
This research was supported by NSF grant EAR-1113355 (C. E., S. R., and J. M.), EAR-1654518 (J. M.), with approval by the Commission for Science and Technology (Tanzania) and the National Council for Science and Technology (Kenya). All seismic data are available through the IRIS Data Management Center. We acknowledge the CoLiBrEA project who sponsored all stations that begin with "PR." We thank N. Lindsey for assistance with the TDMT_INVC method, M. Isken with the Grond software, G. Tepp with the waveform cross correlation, and two anonymous reviewers and Editor L. Flesch for constructive comments that improved this manuscript.

References

Ágústsdóttir, T., Woods, J., Greenfield, T., Green, R. G., White, R. S., Winder, T., et al. (2016). Strike-slip faulting during the 2014 Bárðarbunga-Holuhraun dike intrusion, central Iceland. *Geophysical Research Letters*, *43*, 1495–1503. https://doi.org/10.1002/2015GL067423

Albaric, J., Déverchère, J., Perrot, J., Jakovlev, A., & Deschamps, A. (2014). Deep crustal earthquakes in North Tanzania, East Africa: Interplay between tectonic and magmatic processes in an incipient rift. *Geochemistry, Geophysics, Geosystems*, *15*, 374–394. https://doi.org/10.1002/2013GC005027

Albuquerque Seismological Laboratory (ASL)/USGS (1988). Global Seismograph Network (GSN - IRIS/USGS). International Federation of Digital Seismograph Networks. https://doi.org/10.7914/SN/IU

Alvizuri, C., Silwal, V., Krischer, L., & Tape, C. (2018). Estimation of full moment tensors, including uncertainties, for nuclear explosions, volcanic events, and earthquakes. *Journal of Geophysical Research: Solid Earth*, *123*, 5099–5119. https://doi.org/10.1029/2017JB015325

Ashley, G. M. (2007). Orbital rhythms, monsoons, and playa lake response, Olduvai Basin, equatorial East Africa (ca. 1.85–1.74 Ma). *Geology*, *35*(12), 1091–1094. https://doi.org/10.1130/G24163A.1

Baer, G., Hamiel, Y., Shamir, G., & Nof, R. (2008). Evolution of a magma-driven earthquake swarm and triggering of the nearby Oldoinyo Lengai eruption, as resolved by InSAR, ground observations and elastic modeling, East African Rift, 2007. *Earth and Planetary Science Letters*, *272*(1-2), 339–352. https://doi.org/10.1016/j.epsl.2008.04.052

Belachew, M., Ebinger, C., & Coté, D. (2013). Source mechanisms of dike-induced earthquakes in the Dabbahu-Manda Hararo rift segment in Afar, Ethiopia: Implications for faulting above dikes. *Geophysical Journal International*, *192*(3), 907–917. https://doi.org/10.1093/gji/ggs076

Belachew, M., Ebinger, C., Coté, D., Keir, D., Rowland, J. V., Hammond, J. O. S., & Ayele, A. (2011). Comparison of dike intrusions in an incipient seafloor-spreading segment in Afar, Ethiopia: Seismicity perspectives. *Journal of Geophysical Research*, *116*, B06405. https://doi.org/10.1029/2010JB007908

Biggs, J., Amelung, F., Gourmelen, N., Dixon, T. H., & Kim, S.-W. (2009). InSAR observations of 2007 Tanzania rifting episode reveal mixed fault and dyke extension in an immature continental rift. *Geophysical Journal International*, *179*(1), 549–558. https://doi.org/10.1111/j.1365-246X.2009.04262.x

Biggs, J., Chivers, M., & Hutchinson, M. C. (2013). Surface deformation and stress interactions during the 2007–2010 sequence of earthquake, dyke intrusion and eruption in northern Tanzania. *Geophysical Journal International*, *195*(1), 16–26. https://doi.org/10.1093/gji/ggt226

Birt, C. S., Maguire, P. K. H., Khan, M. A., Thybo, H., Keller, G. R., & Patel, J. (1997). The influence of pre-existing structures on the evolution of the southern Kenya Rift Valley—Evidence from seismic and gravity studies. *Tectonophysics*, *278*(1-4), 211–242. https://doi.org/10.1016/s0040-1951(97)00105-4

Bonafede, M., & Danesi, S. (1997). Near-field modifications of stress induced by dyke injection at shallow depth. *Geophysical Journal International*, *130*(2), 435–448. https://doi.org/10.1111/j.1365-246X.1997.tb05659.x

Brocher, T. M. (2005). Empirical relations between elastic wavespeeds and density in the Earth's crust. *Bulletin of the Seismological Society of America*, *95*(6), 2081–2092. https://doi.org/10.1785/0120050077

Calais, E., d'Oreye, N., Albaric, J., Deschamps, A., Delvaux, D., Déverchère, J., et al. (2008). Strain accommodation by slow slip and dyking in a youthful continental rift, East Africa. *Nature*, *456*(7223), 783–787. https://doi.org/10.1038/nature07478

Cesca, S., Heimann, S., Kriegerowski, M., Saul, J., & Dahm, T. (2017). Moment tensor inversion for nuclear explosions: What can we learn from the 6 January and 9 September 2016 nuclear tests, North Korea? *Seismological Research Letters*, *88*(2A), 300–310. https://doi.org/10.1785/0220160139

Dahm, T., Heimann, S., Funke, S., Wendt, S., Rappsilber, I., Bindi, D., et al. (2018). Seismicity in the block mountains between Halle and Leipzig, Central Germany: Centroid moment tensors, ground motion simulation, and felt intensities of two $M \approx 3$ earthquakes in 2015 and 2017. *Journal of Seismology*, *22*(4), 985–1003. https://doi.org/10.1007/s10950-018-9746-9

Dahm, T., & Krüger, F. (2014). Moment tensor inversion and moment tensor interpretation. In P. Bormann (Ed.), *New Manual of Seismological Observatory Practice NMSOP-2* (pp. 1–37). Potsdam: Deutsches GeoForschungsZentrum GFZ.

Dreger, D. S. (2003). 85.11-TDMT_INV: Time Domain Seismic Moment Tensor INVersion. *International Geophysics*, *81*, 1627. https://doi.org/10.1016/s0074-6142(03)80290-5

Ebinger, C., Djomani, Y. P., Mbede, E., Foster, A., & Dawson, J. B. (1997). Rifting Archaean lithosphere: The Eyasi–Manyara–Natron rifts, East Africa. *Journal of the Geological Society*, *154*, 947–960. https://doi.org/10.1144/gsjgs.154.6.0947

Ebinger, C. J., & Casey, M. (2001). Continental breakup in magmatic provinces: An Ethiopian example. *Geology*, *29*(6), 527–530. https://doi.org/10.1130/0091-7613(2001)029<0527:CBIMPA>2.0.CO;2

Ebinger, C. J., van Wijk, J., & Keir, D. (2013). The time scales of continental rifting: Implications for global processes. In *The Web of Geological Sciences: Advances, Impacts, and Interactions* (Vol. 500, pp. 371–396). America: Geological Society. https://doi.org/10.1130/2013.2500(11)

Efron, B. (1992). Jackknife-after-bootstrap standard errors and influence functions. *Journal of the Royal Statistical Society, Series B*, *54*(1), 83–127. https://doi.org/10.2307/2345949

Ekström, G., Nettles, M., & Dziewonski, A. M. (2012). The global CMT project 2004–2010: Centroid-moment tensors for 13,017 earthquakes. *Physics of the Earth and Planetary Interiors*, *200-201*, 1–9. https://doi.org/10.1016/j.pepi.2012.04.002

Ford, S. R., Dreger, D. S., & Walter, W. R. (2009). Identifying isotropic events using a regional moment tensor inversion. *Journal of Geophysical Research*, *114*, B01306. https://doi.org/10.1029/2008JB005743

Heimann, S., Isken, M., Kühn, D., Sudhaus, H., Steinberg, A., Vasyura-Bathke, H., et al. (2018). Grond—A probabilistic earthquake source inversion framework. V. 1.0. GFZ Data Services. https://doi.org/10.5880/GFZ.2.1.2018.003

Heimann, S., Kriegerowski, M., Isken, M., Cesca, S., Daout, S., Grigoli, F., et al. (2017). Pyrocko—An open-source seismology toolbox and library. https://doi.org/10.5880/GFZ.2.1.2017.001

Jost, M. L., & Herrmann, R. B. (1989). A student's guide to and review of moment tensors. *Seismological Research Letters*, *60*(2), 37–57. https://doi.org/10.1785/gssrl.60.2.37

Keir, D., Ebinger, C. J., Stuart, G. W., Daly, E., & Ayele, A. (2006). Strain accommodation by magmatism and faulting as rifting proceeds to breakup: Seismicity of the northern Ethiopian rift. *Journal of Geophysical Research*, *111*, B05314. https://doi.org/10.1029/2005JB003748

Kervyn, M., Ernst, G. G. J., Keller, J., Vaughan, R. G., Klaudius, J., Pradal, E., et al. (2010). Fundamental changes in the activity of the natrocarbonatite volcano Oldoinyo Lengai, Tanzania. *Bulletin of Volcanology*, *72*(8), 913–931. https://doi.org/10.1007/s00445-010-0360-0

Lee, H., Muirhead, J. D., Fischer, T. P., Ebinger, C. J., Kattenhorn, S. A., Sharp, Z. D., & Kianji, G. (2016). Massive and prolonged deep carbon emissions associated with continental rifting. *Nature Geoscience*, *9*(2), 145–149. https://doi.org/10.1038/ngeo2622

Magee, C., Muirhead, J. D., Karvelas, A., Holford, S. P., Jackson, C. A. L., Bastow, I. D., et al. (2016). Lateral magma flow in mafic sill complexes. *Geosphere*, *12*(3), 809–841. https://doi.org/10.1130/GES01256.1

Mana, S., Furman, T., Carr, M. J., Mollel, G. F., Mortlock, R. A., Feigenson, M. D., et al. (2012). Geochronology and geochemistry of the Essimingor volcano: Melting of metasomatized lithospheric mantle beneath the North Tanzanian Divergence zone (East African Rift). *Lithos*, *155*, 310–325. https://doi.org/10.1016/j.lithos.2012.09.009

Mana, S., Furman, T., Turrin, B. D., Feigenson, M. D., & Swisher, C. C. (2015). Magmatic activity across the East African North Tanzanian Divergence Zone. *Journal of the Geological Society*, *172*(3), 368–389. https://doi.org/10.1144/jgs2014-072

Marone, C., Vidale, J. E., & Ellsworth, W. L. (1995). Fault healing inferred from time dependent variations in source properties of repeating earthquakes. *Geophysical Research Letters*, *22*(22), 3095–3098. https://doi.org/10.1029/95GL03076

McNutt, S. R. (2005). Volcanic seismology. *Annual Review of Earth and Planetary Sciences*, *33*(1), 461–491. https://doi.org/10.1146/annurev.earth.33.092203.122459

Minson, S. E., & Dreger, D. S. (2008). Stable inversions for complete moment tensors. *Geophysical Journal International*, *174*(2), 585–592. https://doi.org/10.1111/j.1365-246X.2008.03797.x

Minson, S. E., Dreger, D. S., Bürgmann, R., Kanamori, H., & Larson, K. M. (2007). Seismically and geodetically determined nondouble-couple source mechanisms from the 2000 Miyakejima volcanic earthquake swarm. *Journal of Geophysical Research*, *112*, B10308. https://doi.org/10.1029/2006JB004847

Modisi, M. P., Atekwana, E. A., Kampunzu, A. B., & Ngwisanyi, T. H. (2000). Rift kinematics during the incipient stages of continental extension: Evidence from the nascent Okavango rift basin, northwest Botswana. *Geology*, *28*(10), 939–942. https://doi.org/10.1130/0091-7613(2000)028<0939:RKDTIS>2.3.CO;2

Muirhead, J. D., Kattenhorn, S. A., & Le Corvec, N. (2015). Varying styles of magmatic strain accommodation across the East African Rift. *Geochemistry, Geophysics, Geosystems*, *16*, 2775–2795. https://doi.org/10.1002/2015GC005918

Muirhead, J. D., Kattenhorn, S. A., Lee, H., Mana, S., Turrin, B. D., Fischer, T. P., et al. (2016). Evolution of upper crustal faulting assisted by magmatic volatile release during early-stage continental rift development in the East African Rift. *Geosphere*, *12*(6), 1670–1700. https://doi.org/10.1130/GES01375.1

Nettles, M., & Ekström, G. (1998). Faulting mechanism of anomalous earthquakes near Bárdarbunga Volcano, Iceland. *Journal of Geophysical Research*, *103*(B8), 17,973–17,983. https://doi.org/10.1029/98JB01392

Panza, G. F., & Saraò, A. (2000). Monitoring volcanic and geothermal areas by full seismic moment tensor inversion: Are non-double-couple components always artefacts of modelling? *Geophysical Journal International*, *143*(2), 353–364. https://doi.org/10.1046/j.1365-246X.2000.01250.x

Pasyanos, M. E., Dreger, D. S., & Romanowicz, B. (1996). Toward real-time estimation of regional moment tensors. *Bulletin of the Seismological Society of America*, *86*(5), 1255–1269.

Plasman, M., Tiberi, C., Ebinger, C., Gautier, S., Albaric, J., Peyrat, S., et al. (2017). Lithospheric low-velocity zones associated with a magmatic segment of the Tanzanian Rift, East Africa. *Geophysical Journal International*, *210*(1), 465–481. https://doi.org/doi.org/10.1093/gji/ggx177

Reyes, C. G., & West, M. E. (2011). The waveform suite: A robust platform for manipulating waveforms in MATLAB. *Seismological Research Letters*, *82*(1), 104–110. https://doi.org/10.1785/gssrl.82.1.104

Roecker, S., Ebinger, C., Tiberi, C., Mulibo, G., Ferdinand-Wambura, R., Mtelela, K., et al. (2017). Subsurface images of the Eastern Rift, Africa, from the joint inversion of body waves, surface waves and gravity: Investigating the role of fluids in early-stage continental rifting. *Geophysical Journal International*, *210*(2), 931–950. https://doi.org/10.1093/gji/ggx220

Rowland, J. V., Baker, E., Ebinger, C. J., Keir, D., Kidane, T., Biggs, J., et al. (2007). Fault growth at a nascent slow-spreading ridge: 2005 Dabbahu rifting episode, Afar. *Geophysical Journal International*, *171*(3), 1226–1246. https://doi.org/10.1111/j.1365-246X.2007.03584.x

Rubin, A. M. (1995). Propagation of magma-filled cracks. *Annual Review of Earth and Planetary Sciences*, *23*(1), 287–336. https://doi.org/10.1146/annurev.earth.23.1.287

Rubin, D. B. (1981). The Bayesian bootstrap. *The Annals of Statistics*, *9*(1), 130–134. https://doi.org/10.2307/2240875
Saikia, C. K. (1994). Modified frequency-wavenumber algorithm for regional seismograms using Filon's quadrature: Modelling of Lg waves in eastern North America. *Geophysical Journal International*, *118*(1), 142–158. https://doi.org/10.1111/j.1365-246X.1994.tb04680.x
Saria, E., Calais, E., Altamimi, Z., Willis, P., & Farah, H. (2013). A new velocity field for Africa from combined GPS and DORIS space geodetic Solutions: Contribution to the definition of the African reference frame (AFREF). *Journal of Geophysical Research: Solid Earth*, *118*, 1677–1697. https://doi.org/10.1002/jgrb.50137
Saria, E., Calais, E., Stamps, D. S., Delvaux, D., & Hartnady, C. J. H. (2014). Present-day kinematics of the East African Rift. *Journal of Geophysical Research: Solid Earth*, *119*, 3584–3600. https://doi.org/10.1002/2013JB010901
Shuler, A., Ekstroem, G., & Nettles, M. (2013). Physical mechanisms for vertical-CLVD earthquakes at active volcanoes. *Journal of Geophysical Research: Solid Earth*, *118*, 1569–1586. https://doi.org/10.1002/jgrb.50131
Silwal, V., & Tape, C. (2016). Seismic moment tensors and estimated uncertainties in southern Alaska. *Journal of Geophysical Research: Solid Earth*, *121*, 2772–2797. https://doi.org/10.1002/2015JB012588
Stähler, S., & Sigloch, K. (2014). Fully probabilistic seismic source inversion—Part 1: Efficient parameterisation. *Solid Earth*, *5*(2), 1055–1069. https://doi.org/10.5194/se-5-1055-2014
Tape, W., & Tape, C. (2013). The classical model for moment tensors. *Geophysical Journal International*, *195*(3), 1701–1720. https://doi.org/10.1093/gji/ggt302
Tepp, G., Ebinger, C. J., & Yun, S. H. (2016). Spectral analysis of dike-induced earthquakes in Afar, Ethiopia. *Journal of Geophysical Research: Solid Earth*, *121*, 2560–2574. https://doi.org/10.1002/2015JB012658
Waldhauser, F., Ellsworth, W. L., Schaff, D. P., & Cole, A. (2004). Streaks, multiplets, and holes: High-resolution spatio-temporal behavior of Parkfield seismicity. *Geophysical Research Letters*, *31*, L18608. https://doi.org/10.1029/2004GL020649
Wang, R. (1999). A simple orthonormalization method for stable and efficient computation of Green's functions. *Bulletin of the Seismological Society of America*, *89*(3), 733–741.
Wauthier, C. (2011). Radar interferometry (InSAR) applied to the study of active volcanic and seismic areas in Africa, PhD dissertation, 245 pp., Univ. of Leige, Liege, Germany.
Wauthier, C., Smets, B., & Keir, D. (2015). Diking-induced moderate-magnitude earthquakes on a youthful rift border fault: The 2002 Nyiragongo-Kalehe sequence, DR Congo. *Geochemistry, Geophysics, Geosystems*, *16*, 4280–4291. https://doi.org/10.1002/2015GC006110
Wauthier, C., Stephens, K., Oliva, S. J., Weinstein, A., & Ebinger, C. J. (2016). Magmatic fluid processes revealed by a joint analysis of seismic and InSAR data in an early continental rift. In *AGU Fall Meeting Abstracts*.
Weinstein, A., Oliva, S. J., Ebinger, C. J., Roecker, S., Tiberi, C., Aman, M., et al. (2017). Fault-magma interactions during early continental rifting: Seismicity of the Magadi-Natron-Manyara basins, Africa. *Geochemistry, Geophysics, Geosystems*, *18*, 3662–3686. https://doi.org/10.1002/2017GC007027